

A Nonconvex Projection Method for Robust PCA

Aritra Dutta ^{*} Filip Hanzely [†] Peter Richtárik [‡]

Abstract

Robust principal component analysis (RPCA) is a well-studied problem whose goal is to decompose a matrix into the sum of low-rank and sparse components. In this paper, we propose a nonconvex feasibility reformulation of RPCA problem and apply an alternating projection method to solve it. To the best of our knowledge, this is the first paper proposing a method that solves RPCA problem without considering any objective function, convex relaxation, or surrogate convex constraints. We demonstrate through extensive numerical experiments on a variety of applications, including shadow removal, background estimation, face detection, and galaxy evolution, that our approach matches and often significantly outperforms current state-of-the-art in various ways.

Principal component analysis (PCA) [34] addresses the problem of best approximation of a matrix $A \in \mathbb{R}^{m \times n}$ by a matrix of rank r :

$$X^* = \arg \min_{\substack{X \in \mathbb{R}^{m \times n} \\ \text{rank}(X) \leq r}} \|A - X\|_F^2, \quad (1)$$

where $\|\cdot\|_F$ denotes the Frobenius norm of matrices. The solution to (1) is given by

$$X^* = H_r(A) \stackrel{\text{def}}{=} U \Sigma_r V^T, \quad (2)$$

where A has singular value decompositions $A = U \Sigma V^T$, and $\Sigma_r(A)$ is the diagonal matrix obtained from Σ by hard-thresholding that keeps the r largest singular values only and replaces the other singular values by 0. In many real-world problems, if sparse large errors or outliers are present in the data matrix, PCA fails to deal with it. Therefore, it is natural to consider a *robust* matrix decomposition model in which we wish to decompose A into the sum of a low-rank matrix L and an error matrix S : $A = L + S$. However, without further assumptions, the problem is ill-posed. We assume that the error matrix S is *sparse* and that it allows its entries to have arbitrarily large magnitudes. That is, given A , we consider the problem of finding a low rank matrix L and a sparse matrix S such that

$$A = L + S. \quad (3)$$

^{*}Division of Computer, Electrical and Mathematical Sciences and Engineering (CEMSE), King Abdullah University of Science and Technology (KAUST), Thuwal, Saudi Arabia, e-mail: aritra.dutta@kaust.edu.sa.

[†]Division of Computer, Electrical and Mathematical Sciences and Engineering (CEMSE), King Abdullah University of Science and Technology (KAUST), Thuwal, Saudi Arabia, e-mail: filip.hanzely@kaust.edu.sa.

[‡]Division of Computer, Electrical and Mathematical Sciences and Engineering (CEMSE), King Abdullah University of Science and Technology (KAUST), Kingdom of Saudi Arabia, e-mail: peter.richtarik@kaust.edu.sa — School of Mathematics, University of Edinburgh, United Kingdom, e-mail: peter.richtarik@ed.ac.uk — Moscow Institute of Physics and Technology, Dolgoprudny, Russia

In this context, the celebrated principal component pursuit (PCP) formulation of the problem uses the ℓ_0 norm (cardinality) to address the sparsity constraint and (3). Therefore, PCP is the constrained minimization problem [11, 15]:

$$\min_{L,S} \text{rank}(L) + \lambda \|S\|_{\ell_0} \quad \text{subject to} \quad A = L + S, \quad (4)$$

where $\lambda > 0$ is a balancing parameter. Since both $\text{rank}(L)$ and $\|S\|_{\ell_0}$ are non-convex, one often replaces the rank function by the (convex) nuclear norm and ℓ_0 by the (convex) ℓ_1 norm. This replacement leads to the immensely popular *robust principal component analysis (RPCA)* [56, 41, 11], which can be seen as a convex relaxation of (4):

$$\min_{L,S} \|L\|_* + \lambda \|S\|_{\ell_1} \quad \text{subject to} \quad A = L + S, \quad (5)$$

where $\|\cdot\|_*$ denotes the nuclear norm (sum of the singular values) of matrices. Under some reasonable assumptions on the low-rank and sparse components, [15, 11] showed that (4) can be provably solved via (5). A vast literature is dedicated to solving the RPCA problem, and among them the exact and inexact augmented Lagrangian method of multipliers [41], accelerated proximal gradient method [56], alternating direction method [59], alternating projection with intermediate denoising [47], dual approach [42], and SpaRCS [55] are a few popular ones. Recently, Yi et al. [58], Zhang and Yang [60] proposed a manifold optimization to solve RPCA. We refer the reader to [6] for a comprehensive review of the RPCA algorithms. However, besides formulation (5), other tractable reformulations of (4) exist as well. For instance, by relaxing the equality constraint in (4) and moving it to the objective as a penalty, together with adding explicit constraints on the target rank r and target sparsity s leads to the following formulation [61]:

$$\begin{aligned} & \min_{L,S} \|A - L - S\|_F^2 \\ & \text{subject to} \quad \text{rank}(L) \leq r \quad \text{and} \quad \|S\|_0 \leq s. \end{aligned} \quad (6)$$

One can extend the above model to the case of partially observed data that leads to the *robust matrix completion (RMC)* problem [16, 53, 17]:

$$\begin{aligned} & \min_{L,S} \|\mathcal{P}_\Omega(A - L - S)\|_F^2 \\ & \text{subject to} \quad \text{rank}(L) \leq r \quad \text{and} \quad \|\mathcal{P}_\Omega(S)\|_0 \leq s', \end{aligned} \quad (7)$$

where $\Omega \subseteq [m] \times [n]$ is the set of observed data entries, and \mathcal{P}_Ω is the restriction operator defined by

$$(\mathcal{P}_\Omega[X])_{ij} = \begin{cases} X_{ij} & (i,j) \in \Omega \\ 0 & \text{otherwise.} \end{cases}$$

We note that with some modifications, problem (6) is contained in the larger class of problem presented by (7). We also refer to some recent work on RMC problem or outlier based PCA in [18, 17]. An extended model of (5) can also be referred to as a more general problem as in [53] (see problem (1.2) in [53]). More specifically, when $\Omega = [m] \times [n]$, that is, the whole matrix is observed, then (7) is (6). One can also think of the matrix completion (MC) problem as a special case of (7) [12, 33, 10, 32, 13, 36, 14, 43]. For MC problems, $S = 0$. Therefore, (7) is a generalization of two fundamental problems: RPCA and RMC.

Contributions. We solved the RPCA and RMC problems by addressing the original decomposition problem (3) directly, without introducing any optimization objective or surrogate constraints. This is a novel approach because we aim to find a point at the intersection of three sets, two of which are non-convex. We formulate both RPCA and RMC as set feasibility problems and propose alternating projection algorithm to solve them. This leads to Algorithm 2 and 3. Our approach is described in the next section. We also propose a convergence analysis of our algorithm.

Our feasibility approach does not require one to use the hard to interpret parameters (such as λ) and surrogate functions (such as the nuclear norm, or ℓ_1 norm) which makes our approach unique compared to existing models. Instead, we rely on two direct parameters: the target rank r and the desired level of sparsity s . By performing extensive numerical experiments on both synthetic and real datasets, we show that our approach can match or outperform state-of-the-art methods in solving the RPCA and RMC problems. More precisely, when the sparsity level is low, our feasibility approach can viably reconstruct any target low rank, which the RPCA algorithms can not. Moreover, our approach can tolerate denser outliers than can the state-of-the-art RPCA algorithms when the original matrix has a low-rank structure (see details in the experiment section). These attributes make our approach attractive to solve many real-world problems because our performance matches or outperforms that of state-of-the-art RPCA algorithms in solution quality, and do this in comparable or less time.

1 Nonconvex Feasibility and Alternating Projections

Set feasibility problem aims to find a point in the intersection of a collection of closed sets, that is:

$$\text{Find } x \in \mathcal{X} \quad \text{where} \quad \mathcal{X} \stackrel{\text{def}}{=} \bigcap_i^m \mathcal{X}_i \neq \emptyset, \quad (8)$$

for closed sets \mathcal{X}_i . Usually, sets \mathcal{X}_i s are assumed to be simple and easy to project on. A special case of the above setting for convex sets \mathcal{X}_i is the convex feasibility problem and is already well studied. In particular, a very efficient convex feasibility algorithm is known as the alternating projection algorithm [35, 4], in which each iteration picks one set \mathcal{X}_i and projects the current iterate on it. There are two main methods to choosing the sets \mathcal{X}_i – traditional cyclic method and randomized method [52, 28, 46], and in general, randomized method is faster and not vulnerable to adversarial set order.

We also note that the alternating projection algorithm for convex feasibility problem does not converge in general to the projection of the starting point onto \mathcal{X} , but rather finds a close-to feasible point in \mathcal{X} , except the case when \mathcal{X}_i s are affine spaces. However, once an exact projection onto \mathcal{X} is desired, Dykstra’s algorithm [7] should be applied.

Algorithm 1: Alternating projection method for set feasibility

```

1 Input      :  $\Pi_i(\cdot)$  – Projector onto  $\mathcal{X}_i$  for each  $i \in \{1, \dots, m\}$ , starting point  $x_0$ 
2 for  $k = 0, 1, \dots$  do
3   |   Choose via some rule  $i$  (e.g., cyclically or randomly)
4   |    $x_{k+1} = \Pi_i(x_k)$ 
   end
5 Output    :  $x_{k+1}$ 

```

On the other hand, for general nonconvex sets \mathcal{X}_i , projection algorithms might not converge. In some special settings, some forms of convergence (for example, local convergence) can be guaranteed even without convexity [39, 38, 31, 19, 48].

1.1 Set feasibility for RPCA

In this scope, we define α -sparsity as it appears in the last convex constraint \mathcal{X}_3 . We do it so that our approach is directly comparable to the approaches from [58, 60]. However, we note that the ℓ_0 -ball constraint can be applied as well.

Definition 1.1 (α -sparsity). *A matrix $S \in \mathbb{R}^{m \times n}$ is considered to be α -sparse if each row and column of S contains at most αn and αm nonzero entries, respectively. That is, the cardinality of the support set of each row and column of the matrix S do not exceed αn and αm , respectively. Formally, we write*

$$\|S_{(i,\cdot)}\|_0 \leq \alpha n \text{ and } \|S_{(\cdot,j)}\|_0 \leq \alpha m \text{ for all } i \in [m], j \in [n],$$

where i^{th} row and j^{th} column of S are $S_{(i,\cdot)}$ and $S_{(\cdot,j)}$, respectively.

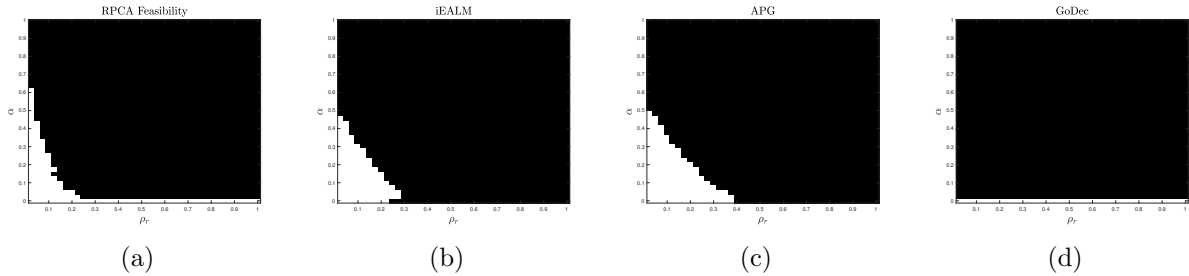


Figure 1: Phase transition diagram for RPCA F, iEALM, APG, and GoDec with respect to rank and error sparsity. Here, $\rho_r = \text{rank}(L)/m$ and α is the sparsity measure. We have $(\rho_r, \alpha) \in (0.025, 1] \times (0, 1)$ with $r = 5 : 5 : 200$ and $\alpha = \text{linspace}(0, 0.99, 40)$. We perform 10 runs of each algorithm.

Now we consider the following reformulation of RPCA:

$$\text{Find } M \stackrel{\text{def}}{=} [L, S] \in \mathcal{X} \stackrel{\text{def}}{=} \bigcap_{i=1}^3 \mathcal{X}_i \neq \emptyset, \quad (9)$$

where

$$\begin{aligned} \mathcal{X}_1 &\stackrel{\text{def}}{=} \{M \mid L + S = A\} \\ \mathcal{X}_2 &\stackrel{\text{def}}{=} \{M \mid \text{rank}(L) \leq r\} \\ \mathcal{X}_3 &\stackrel{\text{def}}{=} \{M \mid \|S_{(i,\cdot)}\|_0 \leq \alpha n \text{ and } \|S_{(\cdot,j)}\|_0 \leq \alpha m \\ &\quad \text{for all } i \in [m], j \in [n].\} \end{aligned} \quad (10)$$

Clearly, \mathcal{X}_1 is convex, but \mathcal{X}_2 and \mathcal{X}_3 are not. Nevertheless, the algorithm we propose – alternating Frobenius norm projection on \mathcal{X}_i performs well to solve RPCA in practice. To validate the robustness of our algorithm, we compare our method to other state-of-the-art RPCA approaches on various practical problems. We also study the local convergence properties and show that despite the non-convex nature of the problem, the algorithms we propose often behave surprisingly well.

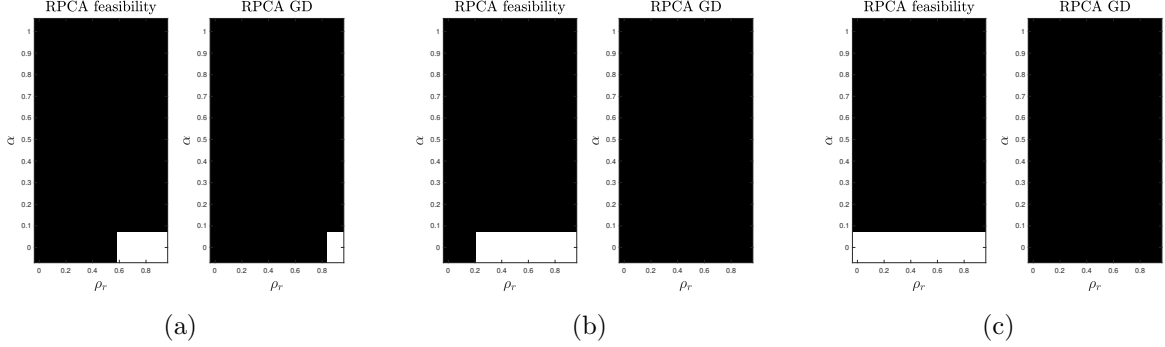


Figure 2: Phase transition diagram for Relative error for RMC problems: (a) $|\Omega^C| = 0.5(m.n)$, (b) $|\Omega^C| = 0.75(m.n)$, (c) $|\Omega^C| = 0.9(m.n)$. Here, $\rho_r = \text{rank}(L)/m$ and α is the sparsity measure. We have $(\rho_r, \alpha) \in (0.025, 1] \times (0, 1)$ with $r = 5 : 25 : 200$ and $\alpha = \text{linspace}(0, 0.99, 8)$.

2 The Algorithm

Denote Π_i to be projector onto \mathcal{X}_i . Note that Π_2 does not include S and projection onto Π_3 does not include L . Consequently, $\Pi_2\Pi_3$ is a projector onto $\mathcal{X}_2 \cap \mathcal{X}_3$. Because our goal is to find a point at the intersection of two sets, we shall employ a cyclic projection method (note that randomized method does not make sense). Indeed, steps 4 and 5 of Algorithm 2 perform projection onto \mathcal{X}_1 , step 6 performs projection onto \mathcal{X}_2 , and finally, step 7 performs projection onto \mathcal{X}_3 . Later in this section we describe the exact implementation and prove correctness the steps mentioned above.

Algorithm 2: Alternating projection method for RPCA

- 1 **Input** : $A \in \mathbb{R}^{m \times n}$ (the given matrix), rank r , sparsity level $\alpha \in (0, 1]$
 - 2 **Initialize**: L_0, S_0
 - 3 **for** $k = 0, 1, \dots$ **do**
 - 4 $\tilde{L} = \frac{1}{2}(L_k - S_k + A)$
 - 5 $\tilde{S} = \frac{1}{2}(S_k - L_k + A)$
 - 6 $L_{k+1} = H_r(\tilde{L})$
 - 7 $S_{k+1} = \mathcal{T}_\alpha(\tilde{S})$
 - end**
 - 8 **Output** : L_{k+1}, S_{k+1}
-

Next, we propose an algorithm to solve the RMC problem (7). Note that we use the generic hard thresholding operator as in (2) in step 6 of Algorithm 3. In practice, however, one can perform cheap SVD.

Finally, we provide a local convergence of Algorithm 2, which depends on the local geometry of the optimal point, and is mostly linear, which we prove later.

Projection on the linear constraint. The next lemma provides an explicit formula for the projection onto \mathcal{X}_1 , which corresponds to steps 4 and 5 of Algorithm 2.

Algorithm 3: Alternating projection method for RMC

1 Input : $A \in \mathbb{R}^{m \times n}$ (the given matrix), rank r , sparsity level $\alpha \in (0, 1]$
2 Initialize: L_0, S_0
3 for $k = 0, 1, \dots$ **do**
4 | $\tilde{L} = \frac{1}{2}\mathcal{P}_\Omega(L_k - S_k + A)$
5 | $\tilde{S} = \frac{1}{2}\mathcal{P}_\Omega(S_k - L_k + A)$
6 | $L_{k+1} = H_r(\tilde{L} + \mathcal{P}_{\Omega^c}(L_k))$
7 | $S_{k+1} = \mathcal{T}_\alpha(\tilde{S})$
end
8 Output : L_{k+1}, S_{k+1}

Lemma 2.1. *Solutions to*

$$\min_{L,S} \|L - L_0\|_F^2 + \|S - S_0\|_F^2 \quad \text{subject to} \quad L + S = A$$

is $L^* = \frac{1}{2}(L_0 - S_0 + A)$ and $S^* = \frac{1}{2}(S_0 - L_0 + A)$.

We also provide an analogy to Lemma 2.1 for the RMC problem (steps 4 and 5 of Algorithm 3).

Lemma 2.2. *Solutions to*

$$\min_{L,S} \|\mathcal{P}_\Omega(L - L_0)\|_F^2 + \|\mathcal{P}_\Omega(S - S_0)\|_F^2 \quad \text{subject to} \quad \mathcal{P}_\Omega(L + S) = \mathcal{P}_\Omega(A)$$

are $L^* = \frac{1}{2}\mathcal{P}_\Omega(L_0 - S_0 + A)$ and $S^* = \frac{1}{2}\mathcal{P}_\Omega(S_0 - L_0 + A)$.

Projection on the low rank constraint. Consider $L^{(r)}$ to be the projection of L onto the rank r constraint, that is,

$$L^{(r)} = \arg \min_{L'} \|L' - L\|_F \quad \text{subject to} \quad \text{rank}(L') \leq r.$$

It is known that $L^{(r)}$ can be computed as r -SVD of L . Fast r -SVD solvers has improved greatly in recent years [29, 45, 50, 1]. Unfortunately, the most recent approaches [50, 1] were not applied in our setting because they are inefficient; they need to compute LL^\top (or $L^\top L$), which is expensive. Instead, we use block Krylov approach from [45]. For completeness, we quote the algorithm in Appendix. Regarding the computational complexity, it was shown that block Krylov SVD outputs Z satisfying $\|L - ZZ^\top L\|_F \leq (1 + \tilde{\epsilon})\|L - L^{(r)}\|_F$ in

$$\mathcal{O} \left(\|L\|_0 \frac{r \log n}{\sqrt{\tilde{\epsilon}}} + \frac{mr^2 \log^2 n}{\tilde{\epsilon}} + \frac{r^3 \log^3 n}{\tilde{\epsilon}^{3/2}} \right)$$

flops. Therefore, projection on the low-rank constraint is not an issue for relatively small rank r .



Figure 3: Background and foreground separation on Stuttgart dataset **Basic** video. Except RPCA GD and our method, all other methods fail to remove the static foreground object.



Figure 4: Background and foreground separation on Stuttgart dataset **Basic** video. We used 90% sample. GRASTA forms a fragmentary background and exhausts around 540 frames to form a stable video. We also note that RPCA GD has more false positives in the foreground.

Projection on sparsity constraint. Projection onto \mathcal{X}_3 simply keeps the α -fraction of the largest elements in absolute value in each row and column and set the rest to zero. One can use a global hard-thresholding operator that considers ℓ_0 constraint on the entire matrix. Instead, we proposed an operator $\mathcal{T}_\alpha(\cdot)$. Indeed, $\mathcal{T}_\alpha(\cdot)$ does not perform an explicit Euclidean projection onto \mathcal{X}_3 . Instead, it performs a projection onto a certain subset of \mathcal{X}_3 and this is clear from the definition (11) (the subset is defined through support Ω_α). Formally, we define:

$$\mathcal{T}_\alpha[S] \stackrel{\text{def}}{=} \mathcal{P}_{\Omega_\alpha}(S) \in \mathbb{R}^{m \times n} : (i, j) \in \Omega_\alpha \text{ if } |S_{ij}| \geq |S_{(i, \cdot)}^{(\alpha n)}| \text{ and } |S_{ij}| \geq |S_{(\cdot, j)}^{(\alpha m)}|, \quad (11)$$

where $S_{(i, \cdot)}^{(\alpha n)}$ and $S_{(\cdot, j)}^{(\alpha m)}$ denote the α fraction of largest entries of S along the i^{th} row and j^{th} column, respectively. This allows us to inexpensively compute an approximate projection onto \mathcal{X}_3 which works well in practice. Remarkably, this does not affect our theoretical results (which are formulated for exact projection onto \mathcal{X}_3) in any way. We note that the operator $\mathcal{T}_\alpha(\cdot)$ is similar to that defined in [58, 60]. Projection on sparsity constraint (11) can be implemented in $\mathcal{O}(nd)$ time: for each row and each column we find αn -th largest element (or αd) and simultaneously (for other rows/columns) mask the rest. In our experiments, we use fast implementation of n -th element computation from [40].

Remark 1. One may use the Douglas-Rachford operator splitting method [2] as an alternative to the nonconvex projections. We leave this for future research.

3 Convergence Analysis

In this section, we establish a local convergence analysis of our algorithm by using the basic properties of the alternating projection algorithm [39]. A similar analysis was done for GoDec [61], although

Algorithm 2 is vastly different compare to GoDec (we report detailed comparison of these algorithms in Appendix).

Recall that Algorithm 1 performs an alternating projection of $[L, S]$ on the sets \mathcal{X}_1 and $\mathcal{X}_\cap \stackrel{\text{def}}{=} \mathcal{X}_2 \cap \mathcal{X}_3$ defined in (10). Before stating the convergence theorem, let us define a (local) angle between sets.

Definition 3.1. *Let a point p be in the intersection of set boundaries ∂K and ∂L . Define $c(K, L, p)$ be the cosine of an angle between sets K and L at point p as:*

$$c(K, L, p) \stackrel{\text{def}}{=} \cos \angle(\partial K^\top|_p, \partial L^\top|_p),$$

where $\partial K^\top|_p$ denotes a tangent space of set boundary ∂K at p and \angle returns the angle between subspaces given as arguments. As a consequence, we have $0 \leq c(K, L, p) \leq 1$.

Let us also define $d_{\mathcal{X}_1 \cap \mathcal{X}_\cap}(x)$ to be an Euclidean distance of a point x to the set $\mathcal{X}_1 \cap \mathcal{X}_\cap$.

Theorem 3.2. [39] *Suppose that $[\bar{L} \ \bar{S}] \in \partial(\mathcal{X}_1 \cap \mathcal{X}_\cap)$. Given any constant $c \in \mathbb{R}$ such that $c > c(\mathcal{X}_1, \mathcal{X}_\cap, [\bar{L} \ \bar{S}])$ there is a starting point $[L_0 \ S_0]$ close to $[\bar{L} \ \bar{S}]$ such that the iterates L_k, S_k of Algorithm 2 satisfy*

$$d_{\mathcal{X}_1 \cap \mathcal{X}_\cap}([L_k \ S_k]) < c^k d_{\mathcal{X}_1 \cap \mathcal{X}_\cap}([L_0 \ S_0]).$$

Remark 2. From Theorem 3.2 it is clear that the smaller $c(\mathcal{X}_1, \mathcal{X}_\cap, [\bar{L} \ \bar{S}])$ produces a faster convergence, while $c(\mathcal{X}_1, \mathcal{X}_\cap, [\bar{L} \ \bar{S}]) = 1$ can stop the convergence, as described in Example 2 in Appendix.

Remark 3. Theorem 3.2 is stated for Algorithm 2, however, one can easily obtain an equivalent result for Algorithm 3 as well.

Remark 4. Considering the nuclear norm relaxation instead of low rank constraint and ℓ_1 norm relaxation instead of sparsity constraint, the set \mathcal{X}_\cap becomes convex, and thus the whole problem becomes convex as well. Therefore, Algorithms 2 and 3 converge globally.

For completeness, we also derive the exact form of tangent spaces of $\mathcal{X}_1, \mathcal{X}_\cap$ mentioned in Definition 3.1. Suppose that $\text{rank}(\bar{L}) = r$, and \bar{S} is a matrix of maximal sparsity, that is, $\bar{S} \in \mathcal{X}_3$ while $\bar{S} + S' \notin \mathcal{X}_3$ s.t. $\|S'\| = 1$ and $\|\bar{S} + S'\|_0 = \|\bar{S}\|_0 + 1$. The tangent spaces of $\partial\mathcal{X}_1$ and $\partial\mathcal{X}_\cap$ at point $[\bar{L} \ \bar{S}]$ are given by

$$\begin{aligned} \partial\mathcal{X}_1^\top|_{[\bar{L} \ \bar{S}]} &= \mathcal{X}_1 \\ \partial\mathcal{X}_\cap^\top|_{[\bar{L} \ \bar{S}]} &= \partial\mathcal{X}_2^\top|_{\bar{L}} \times \partial\mathcal{X}_3^\top|_{\bar{S}}, \end{aligned}$$

where

$$\begin{aligned} \partial\mathcal{X}_2^\top|_{\bar{L}} &= \{\tilde{L} | \tilde{L} = \bar{L} + \tilde{U}\tilde{\Sigma}\tilde{V}^\top, \tilde{U}^\top\tilde{U} = \tilde{V}^\top\tilde{V} = I, \\ &\quad \tilde{U}^\top\tilde{U} = 0, \tilde{V}^\top\tilde{V} = 0, \tilde{\Sigma} = \text{diag} \tilde{\Sigma}\} \\ \partial\mathcal{X}_3^\top|_{\bar{S}} &= \{\tilde{S} | \tilde{S} = \bar{S} + S', S'_{i,j} = 0 \ \forall (i, j) \text{ s.t. } \bar{S}_{i,j} = 0\}. \end{aligned}$$

Later in Appendix, we also empirically show that:

1. Convergence speed is not significantly influenced by starting point.

2. Convergence is usually fastest for small true sparsity level α and small true rank r , which is the situation in many practical applications.
3. Convergence of Algorithm 3 is slower for medium sized number of observable entries, that is, when $|\Omega| \approx 0.5(m \cdot n)$, and faster for smaller and bigger sizes.
4. If sparsity and rank levels (α and r) are set to be smaller than their true values at the optimum incorrectly, Algorithm 2 does not converge (as in this case, $\cap \mathcal{X}_i$ might not exist). Moreover, the performance of the algorithm is sensitive to the choice of r , and this is particularly so if we underestimate the true value (see Figure 8 in Appendix).

Finally, in Appendix we give two examples for the convex version of the problem (9) with the same block structure; in them, the alternating projection algorithm either converges extremely fast or does not even converge linearly.

4 Numerical experiments

To explore the strengths and flexibility of our feasibility approach, we performed numerical experiments. First, we work with synthetic data and subsequently apply our method to four real-world problems.

4.1 Results on synthetic data

To perform our numerical simulations, first, we construct the test matrix A . We follow the seminal work of Wright et al. [56] to design our experiment. To this end, we construct A as a low-rank matrix, L , corrupted by sparse large noise, S , with arbitrary large entries such that $A = L + S$. We generate L as a product of two independent full-rank matrices of size $m \times r$ whose elements are independent and identically distributed (i.i.d.) $\mathcal{N}(0, 1)$ random variables and $\text{rank}(L) = r$. We generate S as a noise matrix whose elements are sparsely supported by using the operator (11) and lie in the range $[-500, 500]$. We fix $m = 200$ and define $\rho_r = \text{rank}(L)/m$ where $\text{rank}(L)$ varies. We choose the sparsity level $\alpha \in (0, 1)$. For each pair of (ρ_r, α) we apply iEALM, APG, and our algorithm to recover the pair (\hat{L}, \hat{S}) such that $\hat{A} = \hat{L} + \hat{S}$ be the recovered matrix. For both APG and iEALM, we set $\lambda = 1/\sqrt{m}$ and for iEALM we use $\mu = 1.25/\|A\|_2$ and $\rho = 1.5$, where $\|A\|_2$ is the spectral norm (maximum singular value) of A . If the recovered matrix pair (\hat{L}, \hat{S}) satisfies the relative error $\frac{\|L - \hat{L}\|_F + \|S - \hat{S}\|_F}{\|A\|_F} < 0.01$ then we consider the construction is viable. In Figure 1 we show the fraction of perfect recovery, where white denotes *success* and black denotes *failure*. As mentioned in [56], the success of APG is approximately below the line $\rho_r + \alpha = 0.35$. However, the success of iEALM is not as good as APG. To conclude, when the sparsity level α is low, our feasibility approach can provide a feasible reconstruction for any ρ_r . We note that for low sparsity level, the RPCA algorithms can only provide a feasible reconstruction for $\rho_r \leq 0.4$. On the other hand, for low ρ_r , our feasibility approach can tolerate sparsity level approximately up to 63%. In contrast, RPCA algorithms can tolerate sparsity up to 50% for low ρ_r . Therefore, taken together, we can argue that our method can be proved useful to solve real-world problems when one wants to recover a moderately sparse matrix having *any* inherent low-rank structure present in it or in case of a low-rank matrix corrupted with dense outliers of arbitrary large magnitudes.

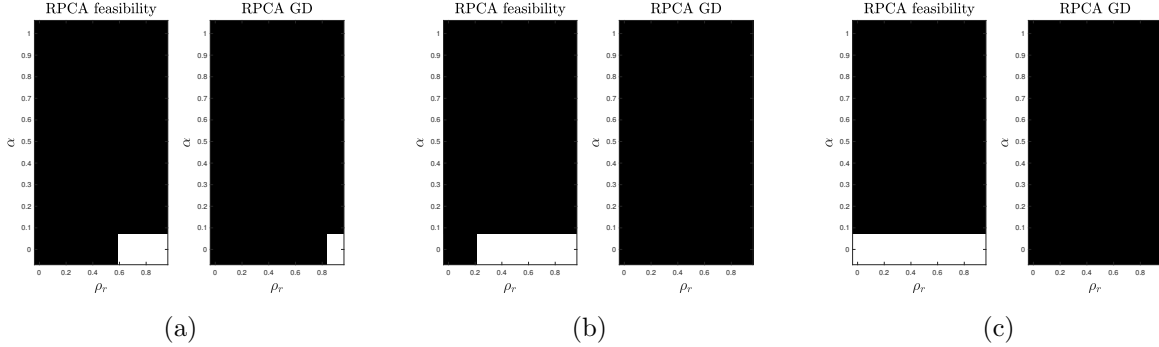


Figure 5: Phase transition diagram for Relative error for RMC problems: (a) $|\Omega^C| = 0.5(m.n)$, (b) $|\Omega^C| = 0.75(m.n)$, (c) $|\Omega^C| = 0.9(m.n)$. Here, $\rho_r = \text{rank}(L)/m$ and α is the sparsity measure. We have $(\rho_r, \alpha) \in (0.025, 1] \times (0, 1)$ with $r = 5 : 25 : 200$ and $\alpha = \text{linspace}(0, 0.99, 8)$.

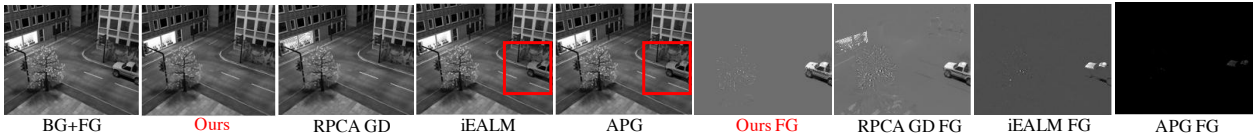


Figure 6: Background and foreground separation on Stuttgart dataset **Basic** video. Except RPCA GD and our method, all other methods fail to remove the static foreground object.

4.2 Results on synthetic data: RMC problem

For experiments in this section, we used a similar technique as in Section 4.1 to generate the test matrix A . We fixed $m = 200$ and denote ρ_r and α same as in Section 4.1. We randomly select the set of observable entries in A . We compare our method against the RPCA gradient descent (RPCA GD) by Yi et al. [58] and use the relative error for the low-rank component recovered as performance measure, that is, if $\|L - \hat{L}\|_F / \|L\|_F < \tilde{\epsilon}$ then we consider the construction is viable. Note that L is the original low-rank matrix and \hat{L} is the low-rank matrix recovered. For $|\Omega^C| = 0.5(m.n)$, $0.75(m.n)$, and $0.9(m.n)$ we consider $\tilde{\epsilon} = 0.2, 0.6$, and 1 , respectively. In Figure 5, for the phase transition diagram white denotes *success* and black denotes *failure*. From Figure 5 we observe that irrespective of the cardinalities of the set of the observed entries our feasibility approach outperforms RPCA GD. However, as the cardinality of the set of the observable entries, that is, $|\Omega|$ decreases, the performance of our feasibility approach gets better (see Figure 5c).

Next, we use the root mean square error (RMSE), that is, $\|L - \hat{L}\|_F / \sqrt{mn}$ as a performance measure for these set of results. Note that L is the original low-rank matrix and \hat{L} is the low-rank matrix recovered. From Figure 7 we observe that when the cardinality of the set of the observable entries Ω is 50% and 75% of $[m] \times [n]$, respectively, RPCA GD has slightly better RMSE than our method as ρ_r increases. However, as the cardinality of the set of the observable entries, that is, $|\Omega|$ decreases, we outperform RPCA GD (see Figure 7c-7d). Therefore, we further validate that for RMC problems, when $|\Omega|$ is small the feasibility approach is better to recover a low-rank matrix.

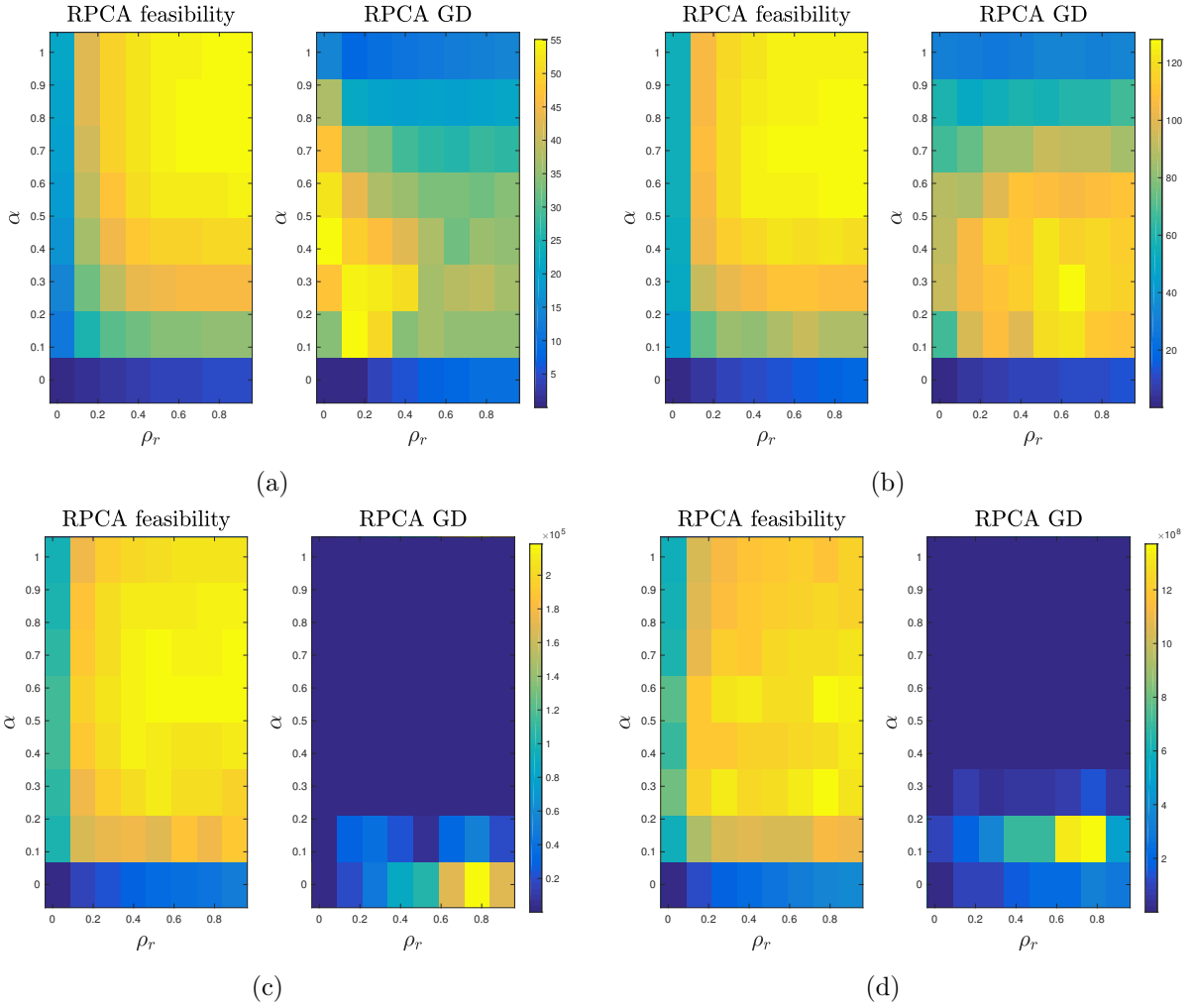


Figure 7: RMSE for RMC problems: (a) $|\Omega^C| = 0.5(m.n)$, (b) $|\Omega^C| = 0.75(m.n)$, (c) $|\Omega^C| = 0.9(m.n)$, (d) $|\Omega^C| = 0.95(m.n)$. Here, $\rho_r = \text{rank}(L)/m$ and α is the sparsity measure. We have $(\rho_r, \alpha) \in (0.025, 1] \times (0, 1)$ with $r = 5 : 25 : 200$ and $\alpha = \text{linspace}(0, 0.99, 8)$.



Figure 8: Background and foreground separation on Stuttgart dataset **Basic** video. We used 90% sample. GRASTA forms a fragmentary background and exhausts around 540 frames to form a stable video. We also note that RPCA GD has more false positives in the foreground.

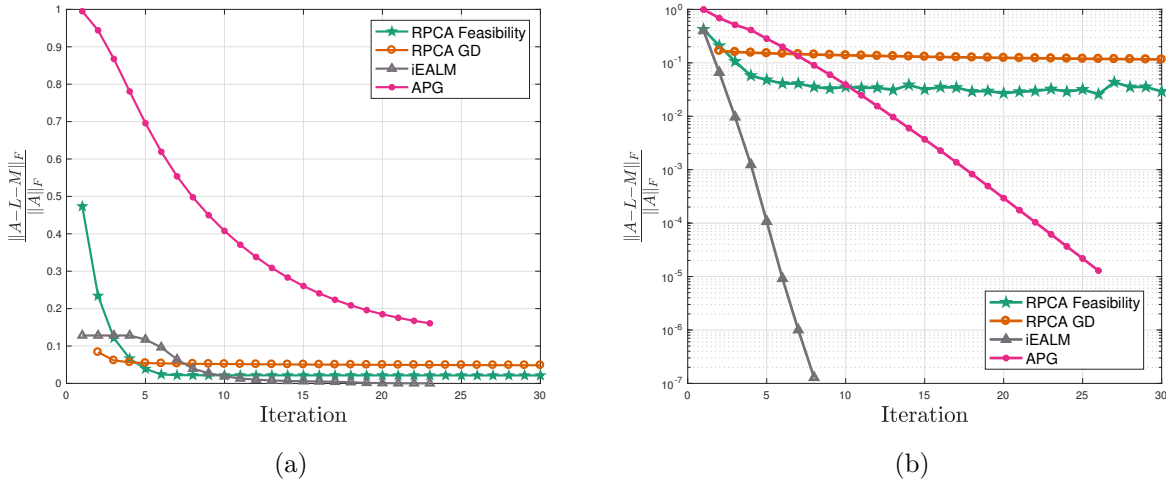


Figure 9: (a) Comparison of relative error vs. iteration between RPCA F, iEALM, APG, and RPCA GD on **Basic** video, frame size 144×176 . iEALM takes 55.41 seconds, RPCA GD takes 36.08 seconds (30 iterations), APG takes 51.14 seconds, and RPCA CF takes 42.72 seconds (30 iterations). The threshold ϵ for all algorithms is set to 2×10^{-4} . (b) Comparison of relative error (log scale) vs. iteration between RPCA F, iEALM, APG, and RPCA GD on Shadow removal, **Yale Extended Face** dataset, subject B12. iEALM takes 2.05 seconds (threshold 10^{-7}), RPCA GD takes 4.73 seconds (30 iterations, threshold 2×10^{-4}), APG takes 10.9 seconds (threshold 10^{-7}), and RPCA CF takes 4.71 seconds (30 iterations, threshold 2×10^{-4}). For APG and iEALM we plot every fifth iteration.

4.3 Applications to real-world problem

In this section we demonstrate the robustness of our feasibility approach to solve four classic real-world problems: i) background and foreground estimation from fully and partially observed data, ii) shadow removal from face images captured under varying illumination and camera position, iii) inlier subspace detection, iv) processing astronomical data.

4.3.1 Background and foreground estimation from fully observed data

In this section, we show our results on the background estimation problem. In the past decade, one of the most prevalent approaches used to solve background estimation problem is to treat it as a low-rank and sparse matrix decomposition problem [5, 51, 21, 44, 54, 30, 57, 20, 23, 24, 22]. Given a sequence of n video frames with each frame mapped into a vector $a_i \in \mathbb{R}^m$, $i = 1, 2, \dots, n$, the data matrix $A \in \mathbb{R}^{m \times n}$ in the collection of all the frame vectors is expected to be split into $L + S$. By using the above idea, RPCA [11, 41, 56] was introduced by considering the background frames, L , having a low-rank structure and the foreground, S , sparse. The convex relaxation of the problem is (5).

For simulations, we used the **Basic** sequence of the Stuttgart artificial dataset [8]. We compare our methods against inexact augmented Lagrange methods of multiplier (iEALM) of Lin et al. [41], accelerated proximal gradient (APG) of Wright et al. [56], and RPCA GD. We downsampled the video frames to a resolution of 144×176 and for iEALM we use $\mu = 1.25/\|A\|_2$ and $\rho = 1.5$. For both APG and iEALM we set $\lambda = 1/\sqrt{\max\{m, n\}}$. For RPCA GD and our method we use target rank $r = 2$, sparsity $\alpha = 0.1$. The threshold ϵ for all methods are kept to 2×10^{-4} . The qualitative

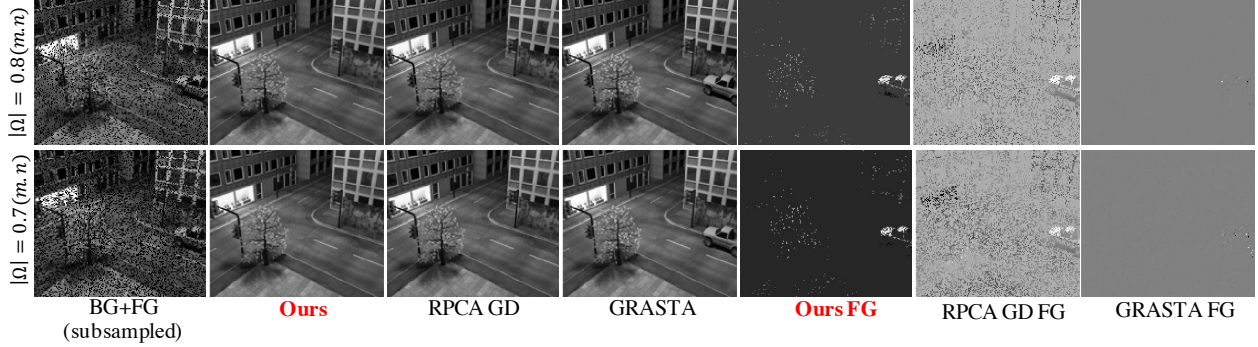


Figure 10: Background and foreground separation on Stuttgart dataset **Basic** video. We used 80% and 70% sample, respectively. GRASTA forms a fragmentary background and exhausts around 540 frames to form a stable video. We also note that RPCA GD has more false positives in the foreground. In contrast our feasibility approach recovers superior quality background and foreground.

analysis on the background and foreground recovered on the sample frame of the **Basic** sequence in Figure 6 suggests that our method and RPC GD recover a visually better quality background and foreground compare with the other methods. We also note that RPCA GD recovers a foreground with more false positives compare to our method and iEALM and APG cannot remove the static foreground object.

4.3.2 Background and foreground estimation from partially observed data

We randomly select the set of observable entries in the data matrix A and tested our algorithm against Grassmannian Robust Adaptive Subspace Tracking Algorithm (GRASTA) [30] and RPCA GD. In Figure 8, we demonstrate the performance on the **Basic** sequence of the Stuttgart dataset with $|\Omega| = 0.9(m.n)$. The parameters for our algorithm and RPCA GD are set as same as in Section 4.3.1. For GRATSAs we set the parameters same as mentioned in the authors’ website¹. Next, in Figure 10 we show the background and foreground separated by different methods on the same sample frame of the **Basic** sequence of Stuttgart dataset for different subsample rate. It is evident that RPCA GD and our approach has the best background reconstruction. However, when compared with the foreground ground truth our method has a better quantitative measure as RPCA GD has a higher number of false positives in the foreground (see Figure 11).

Background and foreground estimation from partially observed data: Quantitative measure. Let $X = (X_1, \dots, X_n)$ and $y = (Y_1, \dots, Y_n)$ be two video sequences (reconstructed foreground and ground truth foreground), where $X_i, Y_i \in \mathbb{R}^m$ are vectors corresponding to frame i , each containing m pixels. We scale all pixel values to $[0, 1]$. To compare the video sequences, we define an ϵ -proximity measure of X and Y as

$$d^\epsilon(X, Y) \stackrel{\text{def}}{=} \frac{1}{nm} \sum_{i=1}^n \sum_{k=1}^m d^\epsilon(X_{ik}, Y_{ik}),$$

¹<https://sites.google.com/site/hejunzz/grasta>

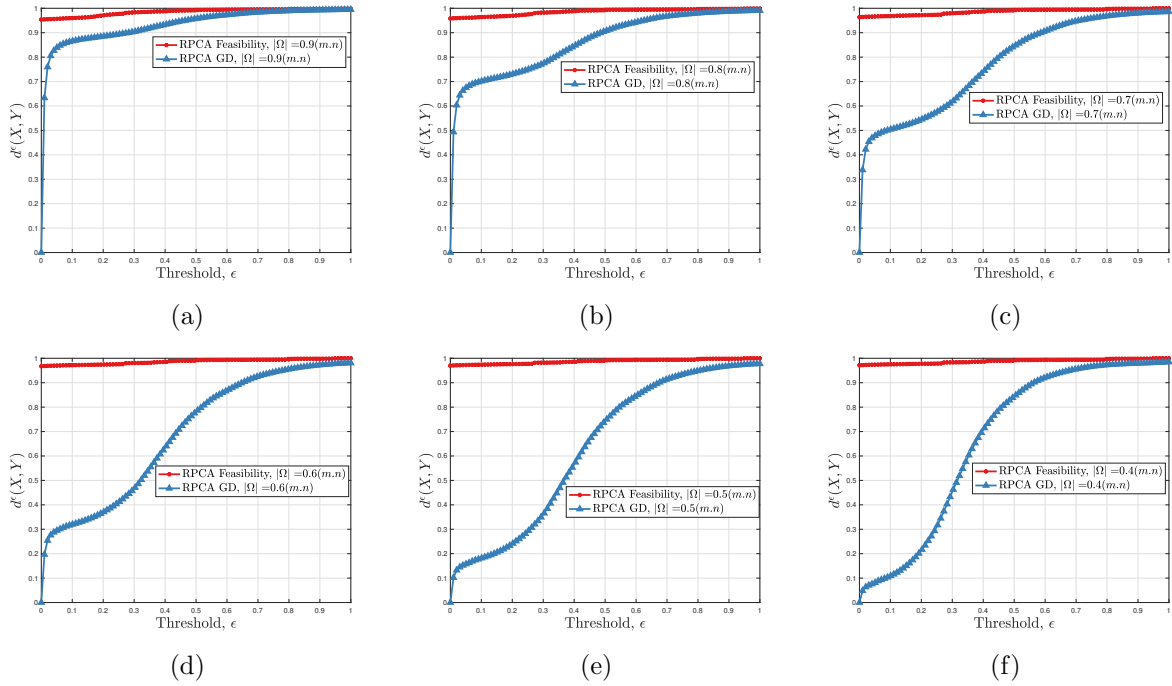


Figure 11: Quantitative comparison of foreground recovered by RPCA GD and RPCA F on Basic video, frame size 144×176 with observable entries: (a) $|\Omega| = 0.9(m.n)$, (b) $|\Omega| = 0.8(m.n)$, (c) $|\Omega| = 0.7(m.n)$, (d) $|\Omega| = 0.6(m.n)$, (e) $|\Omega| = 0.5(m.n)$, and (f) $|\Omega| = 0.4(m.n)$. The performance of RPCA GD drops significantly as $|\Omega|$ decreases. In contrast, the performance of RPCA F stays stable irrespective of the size of $|\Omega|$.

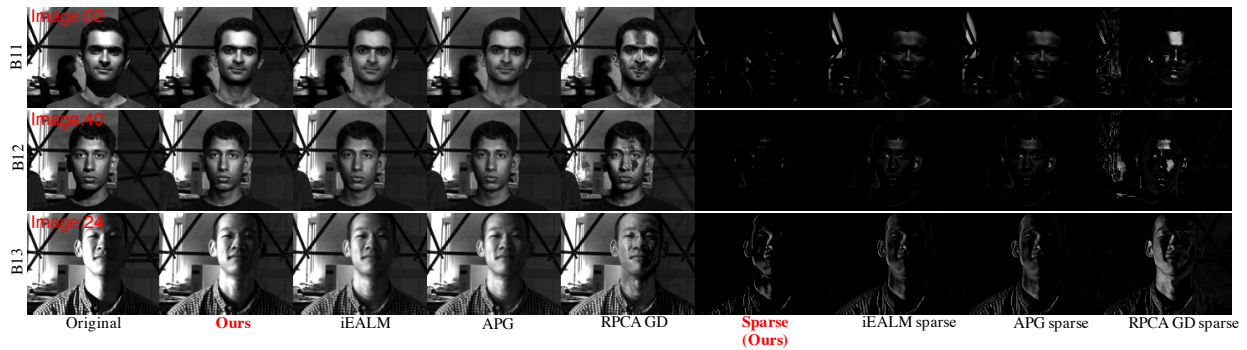


Figure 12: Shadow and specularities removal from face images captured under varying illumination and camera position. Our feasibility approach provides comparable reconstruction to that of iEALM and APG.

where

$$d^\epsilon(u, v) \stackrel{\text{def}}{=} \begin{cases} 1 & |u - v| \leq \epsilon, \\ 0 & \text{otherwise,} \end{cases}$$

and $\epsilon \in [0, 1]$ is a threshold. Clearly, $0 \leq d^\epsilon(X, Y) \leq 1$, $\epsilon \mapsto d^\epsilon(X, Y)$ is increasing, and $d^1(X, Y) = 1$. If $d^\epsilon(X, Y) = \alpha$, then $\alpha \times 100\%$ of pixels in the recovered video are within ϵ distance, in absolute value, from the ground truth.

In Figure 11, we plot $d^\epsilon(X, Y)$ as a function of ϵ for our method and RPCA GD. We use the **Basic** sequence of the Stuttgart dataset and vary the cardinality of the set of observable entries Ω . Our feasibility approach outperforms RPCA GD for all values of $|\Omega|$ and ϵ , and the difference is striking; in particular, our method recovers more than 95% pixels correctly even for under accuracy (i.e., small ϵ) requirements.

4.3.3 Shadow removal

The images of a face exposed to a wide variety of lighting conditions can be approximated accurately by a low-dimensional linear subspace. More specifically, the images under distant, isotropic lighting lie close to a 9-dimensional linear subspace which is known as the harmonic plane [3]. We used the **Extended Yale Face Database** for our experiments [26]. We used iEALM, APG, and RPCA GD to compare against our algorithm. We downsampled each image to a resolution of 120×160 and use 63 images of a subject in each test. For APG and iEALM, we set the parameters same as in Section 4.3.1. For RPCA GD and our method, we set target rank $r = 9$ and sparsity level $\alpha = 0.1$. The qualitative analysis on the recovered images shows that our feasibility approach provides a comparable reconstruction similar to that of iEALM and APG (see Figure 12). In contrast, the reconstructed face images by RPCA GD are of poor visual quality.

4.3.4 Inlier detection

Our next set of experiments demonstrate the power of our method in detecting the inliers and the outliers from a composite dataset. For this purpose, we artificially create a dataset that contains both inliers and outliers. We used the **Yale Extended Face Database** to construct a data set that contains images of faces under different illuminations. We denote this as inliers. With these inliers, we infused 400 random natural images from the **BACKGROUND/Google** folder of the Caltech101 database [25] that serve as outliers. Both inlier and outlier images were converted to grayscale and the resolution is downsampled to 20×20 pixels. For the inliers, we are looking for the 9-dimensional linear subspace where the images of the same face lie. That is, similar to [27] we consider a low-dimensional model to the set of all faces aka inliers. We note that the seven algorithms proposed in [27] are designed to explicitly find a low-rank subspace. In [27] the authors used different objective functions and used SGD, incremental approach, and mirror descent algorithms to find the low-dimensional subspace. However, we approach the problem slightly differently. We split the dataset, A , into a 9-dimensional low-rank subspace L and expect the specularities and outliers to be in the sparse set S . Once we find L , we extract the basis of L and project the faces on it. In Figure 13, we show the qualitative results of our experiments².

²The codes and datasets for experiments in Section 4.3.4 and 4.3.5 are obtained from <https://github.com/jwgoes/RSPCA>

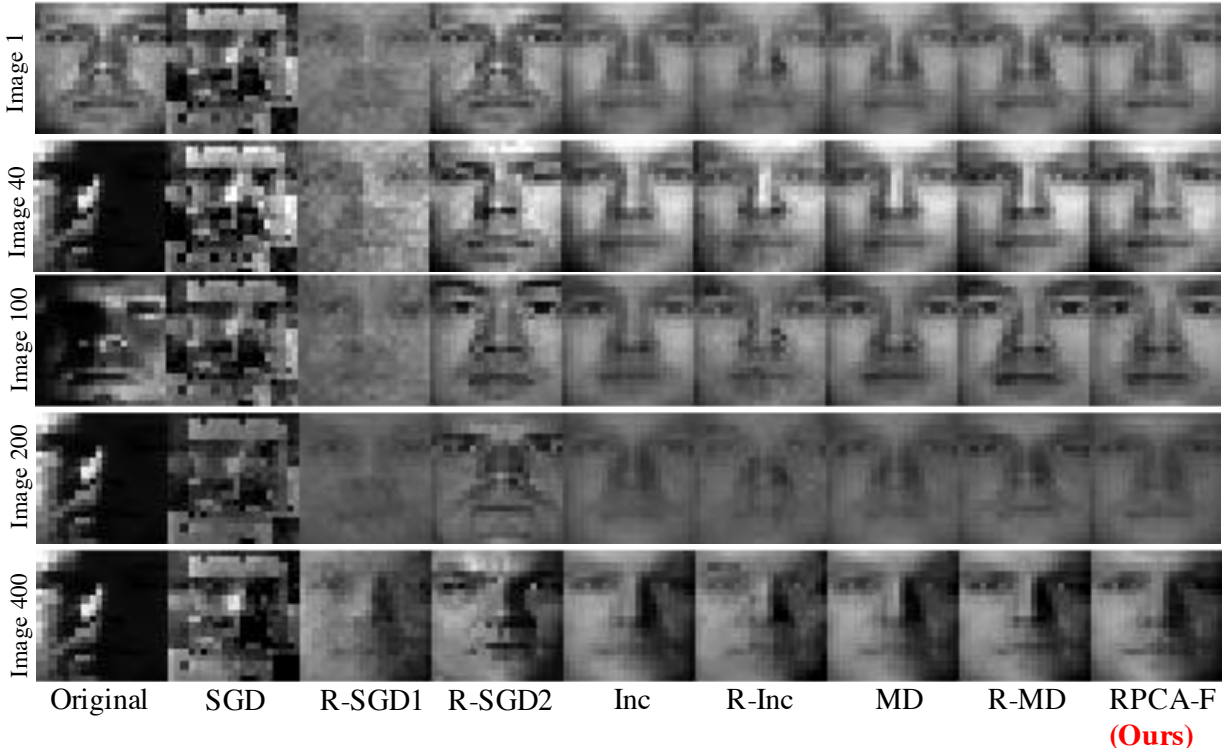


Figure 13: Inliers and outliers detection. Face images captured in different lighting conditions are inliers. We project different faces to 9 dimensional subspaces found by different methods.

Metric used	SGD	R-SGD1	R-SGD2	Inc	R-Inc	MD	R-MD	RPCA-F
$\frac{\ P_L - P_{L^*}\ _F}{3\sqrt{2}}$	0.6985	0.8603	4.6607	0.7703	0.7214	0.6711	0.6679	0.7764

Table 1: Quantitative performance of different algorithms in inlier detection experiment. Except R-SGD2 all methods are highly competitive.

As proposed in [27], we use the error term $\|P_L - P_{L^*}\|_F/3\sqrt{2}$, where L is subspace fitted by the PCA to the set of inliers and L^* be the subspace fitted by different algorithms. We normalize the quantity $\|P_L - P_{L^*}\|_F$ because when $L \perp L^*$, $\|P_L - P_{L^*}\|_F/3\sqrt{2} \approx 1$. Therefore, $\|P_L - P_{L^*}\|_F/3\sqrt{2}$ is expected to lie between 0 and 1 where the smaller is the better. We refer to Table 1 for our quantitative results.

4.3.5 Processing astronomical data

In this experiment, we use the VIMOS Very Large Telescope (VIMOS-VLT) Deep Survey dataset [37] to understand the evolution of the galaxies. We compare the first 4 eigenspectra obtained by our feasibility approach with those of the state-of-the-art methods, such as RE-PCA of [9], online PCA, and robust online PCA of [27]. Similar to Section 4.3.4, we split the dataset, A , into a 4-dimensional low-rank subspace L and after we find L , we extract the orthogonal basis of L and plot them. From Figure 14, visually, robust online PCA and our method are close relatively best fit to the ground

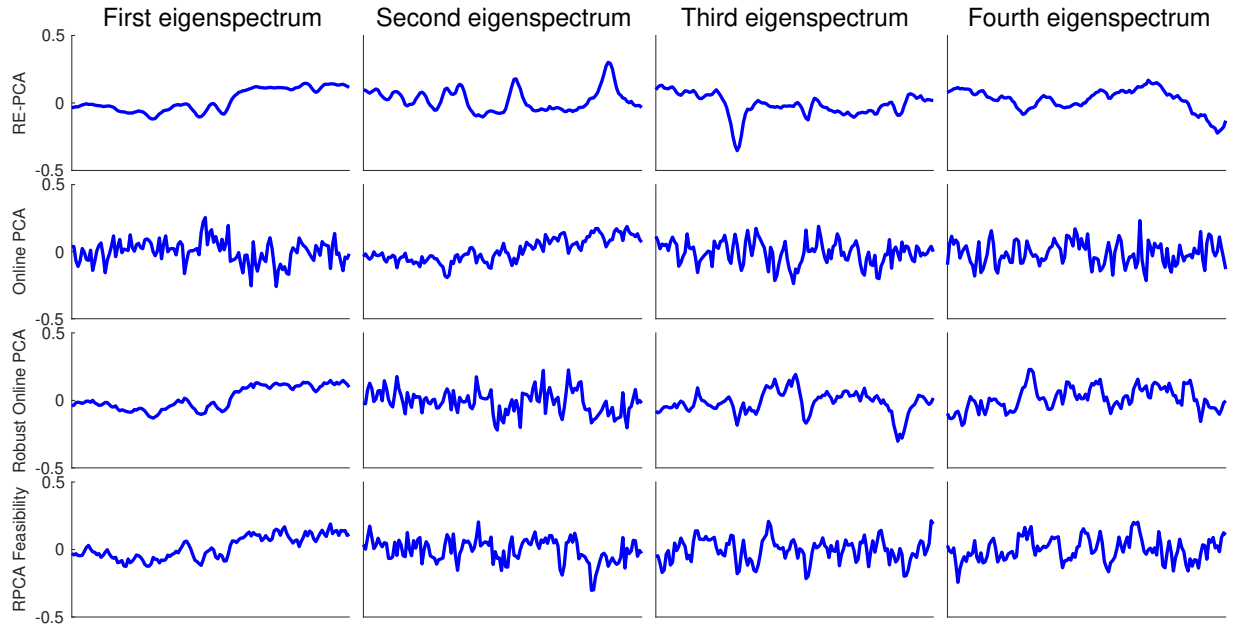


Figure 14: The top four eigenspectra for the VVDS galaxies. The top three rows are the state-of-the art algorithms RE-PCA of [9], online PCA, and robust online PCA of [27], respectively. The last row is our feasibility approach.

truth RE-PCA of [9]. For details of the data, motivation, and experimental setup we refer the readers to [37, 9, 27].

4.4 Further experiments

We show many of our experimental results in the Appendix. On synthetic data, we empirically validate the sensitivity of Algorithm 2 with respect to the initialization, the choices of r , and sparsity level α ; and the effect of the cardinality of Ω for Algorithm 3 (see A.1, A.2, and A.3).

5 Conclusion

In this paper, we propose a simplistic and novel approach to solve the classic RPCA and RMC problems. We consider an alternating projection algorithm based on the set feasibility approach to solve these problems in their crude form, without considering any further heuristics, such as loss functions, convex and surrogate constraints. Although we did not rigorously study convergence of our method theoretically; we investigated the convergence through numerical simulations on synthetic and real-world data and extensively compared with the current state-of-the-art methods. Our feasibility approach can open a new direction of potential research on online algorithms based on RPCA framework [49, 30, 57] that vastly used in video analysis, segmentation, subspace detection, and only a few to mention.

References

- [1] Z. A.-Zhu and Y. Li. LazySVD: Even faster SVD decomposition yet without agonizing pain. In *Advances in Neural Information Processing Systems*, pages 974–982, 2016.
- [2] Francisco J Aragón Artacho, Jonathan M Borwein, and Matthew K Tam. Global behavior of the Douglas–Rachford method for a nonconvex feasibility problem. *Journal of Global Optimization*, 65(2):309–327, 2016.
- [3] R. Basri and D. Jacobs. Lambertian reflection and linear subspaces. *IEEE Transaction on Pattern Analysis and Machine Intelligence*, 25(3):218–233, 2003.
- [4] H. H. Bauschke and J. M. Borwein. On projection algorithms for solving convex feasibility problems. *SIAM review*, 38(3):367–426, 1996.
- [5] T. Bouwmans, A. Sobral, S. Javed, S. K. Jung, and E.-H. Zahzah. Decomposition into low-rank plus additive matrices for background/foreground separation: A review for a comparative evaluation with a large-scale dataset. *Computer Science Review*, 23:1–71, 2017.
- [6] T. Bouwmans and E.-H. Zahzah. Robust PCA via principal component pursuit: A review for a comparative evaluation in video surveillance. *Computer Vision and Image Understanding*, 122:22–34, 2014.
- [7] J. P. Boyle and R. L. Dykstra. A method for finding projections onto the intersection of convex sets in Hilbert spaces. In *Advances in order restricted statistical inference*, pages 28–47. Springer, 1986.
- [8] S. Brutzer, B. Höferlin, and G. Heidemann. Evaluation of background subtraction techniques for video surveillance. *IEEE Computer Vision and Pattern Recognition*, pages 1568–1575, 2012.
- [9] T. Budavari, V. Wild, A. S. Szalay, L. Dobos, and C.-W. Yip. Reliable eigenspectra for new generation surveys. *Monthly Notices of the Royal Astronomical Society*, 394(3):1496–1502, 2009.
- [10] J. F. Cai, E. J. Candès, and Z. Shen. A singular value thresholding algorithm for matrix completion. *SIAM Journal on Optimization*, 20(4):1956–1982, 2010.
- [11] E. J. Candès, X. Li, Y. Ma, and J. Wright. Robust principal component analysis? *Journal of the Association for Computing Machinery*, 58(3):11:1–11:37, 2011.
- [12] E. J. Candès and Y. Plan. Matrix completion with noise. *Proceedings of the IEEE*, 98(6):925–936, 2009.
- [13] E. J. Candès and B. Recht. Exact matrix completion via convex optimization. *Foundations of Computational Mathematics*, 9(6):717–772, 2009.
- [14] E. J. Candès and T. Tao. The power of convex relaxation: Near-optimal matrix completion. *IEEE Transactions on Information Theory*, 56(5):2053–2080, 2010.
- [15] V. Chandrasekaran, S. Sanghavi, P. A. Parrilo, and A. S. Willsky. Rank-sparsity incoherence for matrix decomposition. *SIAM Journal on Optimization*, 21(2):572–596, 2011.
- [16] Y. Chen, H. Xu, C. Caramanis, and S. Sanghavi. Robust matrix completion and corrupted columns. In *Proceedings of the 28th International Conference on International Conference on Machine Learning*, pages 873–880, 2011.
- [17] Y. Cherapanamjeri, K. Gupta, and P. Jain. Nearly optimal robust matrix completion. In *Proceedings of the 34th International Conference on Machine Learning (ICML)*, pages 797–805, 2017.
- [18] Y. Cherapanamjeri, P. Jain, and P. Netrapalli. Thresholding based outlier robust PCA. In *Proceedings of the 30th Conference on Learning Theory (COLT)*, pages 593–628, 2017.
- [19] D. Drusvyatskiy, A. D. Ioffe, and A. S. Lewis. Transversality and alternating projections for nonconvex sets. *Foundations of Computational Mathematics*, 15(6):1637–1651, 2015.

- [20] A. Dutta. *Weighted Low-Rank Approximation of Matrices: Some Analytical and Numerical Aspects*. PhD thesis, University of Central Florida, 2016.
- [21] A. Dutta, B. Gong, X. Li, and M. Shah. Weighted singular value thresholding and its application to background estimation, 2017. arXiv:1707.00133.
- [22] A. Dutta and X. Li. Weighted low rank approximation for background estimation problems. In *The IEEE International Conference on Computer Vision Workshops (ICCVW)*, pages 1853–1861, 2017.
- [23] A. Dutta, X. Li, and P. Richtárik. A batch-incremental video background estimation model using weighted low-rank approximation of matrices. In *The IEEE International Conference on Computer Vision Workshops (ICCVW)*, pages 1835–1843, 2017.
- [24] A. Dutta, X. Li, and P. Richtárik. Weighted low-rank approximation of matrices and background modeling, 2018. arXiv:1804.06252.
- [25] L. Fei-Fei, R. Fergus, and P. Perona. Learning generative visual models from few training examples: An incremental Bayesian approach tested on 101 object categories. *Computer Vision and Image Understanding*, 106(1):59–70, 2007.
- [26] A. Georghiadis, P. Belhumeur, and D. Kriegman. From few to many: Illumination cone models for face recognition under variable lighting and pose. *IEEE Transactions on PAMI*, 23(6):643–660, 2001.
- [27] J. Goes, T. Zhang, R. Arora, and G. Lerman. Robust stochastic principal component analysis. In *Proceedings of the 17th International Conference on Artificial Intelligence and Statistics*, pages 266–274, 2014.
- [28] R. M. Gower and P. Richtárik. Randomized iterative methods for linear systems. *SIAM Journal on Matrix Analysis and Applications*, 36(4):1660–1690, 2015.
- [29] N. Halko, P.-G. Martinsson, and J. A. Tropp. Finding structure with randomness: Probabilistic algorithms for constructing approximate matrix decompositions. *SIAM review*, 53(2):217–288, 2011.
- [30] J. He, L. Balzano, and A. Szlam. Incremental gradient on the Grassmannian for online foreground and background separation in subsampled video. *IEEE Computer Vision and Pattern Recognition*, pages 1937–1944, 2012.
- [31] R. Hesse and D. R. Luke. Nonconvex notions of regularity and convergence of fundamental algorithms for feasibility problems. *SIAM Journal on Optimization*, 23(4):2397–2419, 2013.
- [32] P. Jain and P. Netrapalli. Fast exact matrix completion with finite samples. In *Proceedings of The 28th Conference on Learning Theory (COLT)*, pages 1007–1034, 2015.
- [33] P. Jain, P. Netrapalli, and S. Sanghavi. Low-rank matrix completion using alternating minimization. In *Proceedings of the Forty-fifth Annual ACM Symposium on Theory of Computing*, pages 665–674, 2013.
- [34] I. T. Jolliffe. *Principal component analysis*, 2002. Second edition.
- [35] S. Kaczmarz. Angenaherte auflösung von systemen linearer gleichungen. *Bulletin International de l’Académie Polonaise des Sciences et des Lettres, A*, 35:355–357, 1937.
- [36] R. Keshavan, A. Montanari, and S. Oh. Matrix completion from a few entries. *IEEE Transactions on Information Theory*, 56(6):2980–2998, 2010.
- [37] O. L. Fèvre, G. Vettolani, B. Garilli, L. Tresse, D. B. V. L. Brun, D. Maccagni, J. P. Picat, R. Scaramella, M. Scodeggio, et al. The VIMOS VLT deep survey-First epoch VVDS-deep survey: 11564 spectra with $17 < I(AB) < 24$, and the redshift distribution over $0 < z < 5$. *Astronomy & Astrophysics*, 439(3):845–862, 2005.
- [38] A. S. Lewis, R. Luke, and J. Malick. Local linear convergence for alternating and averaged non-convex projections. *Foundations of Computational Mathematics*, 9(4):485–513, 2009.

- [39] A. S. Lewis and J. Malick. Alternating projections on manifolds. *Mathematics of Operations Research*, 33(1):216–234, 2008.
- [40] P. Li. Nth element. <https://www.mathworks.com/matlabcentral/fileexchange/29453-nth-element>, 2013.
- [41] Z. Lin, M. Chen, and Y. Ma. The augmented Lagrange multiplier method for exact recovery of corrupted low-rank matrices, 2010. arXiv1009.5055.
- [42] Z. Lin, A. Ganesh, J. Wright, L. Wu, M. Chen, and Yi Ma. Fast convex optimization algorithms for exact recovery of a corrupted low-rank matrix. *UIUC Technical Report UILU-ENG-09-2214*, 2009.
- [43] J. Mareček, P. Richtárik, and M. Takáč. Matrix completion under interval uncertainty. *European Journal of Operational Research*, 256(1):35 – 43, 2017.
- [44] G. Mateos and G. Giannakis. Robust PCA as bilinear decomposition with outlier-sparsity regularization. *IEEE Transaction on Signal Processing*, 60(10):5176–5190, 2012.
- [45] C. Musco and C. Musco. Randomized block Krylov methods for stronger and faster approximate singular value decomposition. In *Advances in Neural Information Processing Systems*, pages 1396–1404, 2015.
- [46] I. Necoara, P. Richtárik, and A. Patrascu. Randomized projection methods for convex feasibility problems: conditioning and convergence rates. *arXiv preprint arXiv:1801.04873*, 2018.
- [47] P. Netrapalli, U. N. Niranjan, S. Sanghavi, A. Anandkumar, and P. Jain. Non-convex robust PCA. In *Advances in Neural Information Processing Systems 27*, pages 1107–1115. 2014.
- [48] C. H. J. Pang. Nonconvex set intersection problems: From projection methods to the newton method for super-regular sets. *arXiv:1506.08246*, 2015.
- [49] P. Rodriguez and B. Wohlberg. Incremental principal component pursuit for video background modeling. *Journal of Mathematical Imaging and Vision*, 55(1):1–18, 2016.
- [50] O. Shamir. A stochastic PCA and SVD algorithm with an exponential convergence rate. In *International Conference on Machine Learning*, pages 144–152, 2015.
- [51] A. Sobral and A. Vacavant. A comprehensive review of background subtraction algorithms evaluated with synthetic and real videos. *Computer Vision and Image Understanding*, 122:4 – 21, 2014.
- [52] T. Strohmer and R. Vershynin. A randomized Kaczmarz algorithm with exponential convergence. *Journal of Fourier Analysis and Applications*, 15(2):262, 2009.
- [53] M. Tao and J. Yang. Recovering low-rank and sparse components of matrices from incomplete and noisy observations. *SIAM Journal on Optimization*, 21(1):57–81, 2011.
- [54] N. Wang, T. Yao, J. Wang, and D.-Y. Yeung. A probabilistic approach to robust matrix factorization. In *Proceedings of 12th European Conference on Computer Vision*, pages 126–139, 2012.
- [55] A. E. Waters, A. C. Sankaranarayanan, and R. Baraniuk. SpaRCS: Recovering low-rank and sparse matrices from compressive measurements. *Proceedings of 24th Advances in Neural Information Processing systems*, pages 1089–1097, 2011.
- [56] J. Wright, Y. Peng, Y. Ma, A. Ganesh, and S. Rao. Robust principal component analysis: Exact recovery of corrupted low-rank matrices by convex optimization. *Proceedings of 22nd Advances in Neural Information Processing systems*, pages 2080–2088, 2009.
- [57] J. Xu, V. K. Ithapu, L. Mukherjee, J. M. Rehg, and V. Singh. Gosus: Grassmannian online subspace updates with structured sparsity. In *In Proceedings of IEEE International Conference on Computer Vision*, pages 3376–3383, 2013.
- [58] X. Yi, D. Park, Y. Chen, and C. Caramanis. Fast algorithms for robust PCA via gradient descent. *Advances in Neural Information Processing systems*, pages 361–369, 2016.

- [59] X. Yuan and J. Yang. Sparse and low-rank matrix decomposition via alternating direction methods. *Pacific Journal of Optimization*, 9(1):167–180, 2013.
- [60] T. Zhang and Y. Yang. Robust PCA by manifold optimization, 2017. arXiv:1708.00257v3.
- [61] T. Zhou and D. Tao. Godec: Randomized low-rank and sparse matrix decomposition in noisy case. In *Proceedings of the 28th International Conference on Machine Learning (ICML)*, pages 33–40, 2011.

A Additional Numerical Experiments

In this section we empirically study the convergence of Algorithm 2.

A.1 Algorithm 2: Sensitivity to initialization

First, we examine how the starting point influences the convergence. We construct $A \in \mathbb{R}^{100 \times 100}$ and perform 50 runs of Algorithm 2 for various values of α and r . In all cases, we set

$$A \stackrel{\text{def}}{=} \mathcal{T}_\alpha(S') + H_r(L')$$

for S', L' with independent random entries from $\mathcal{N}(0, 1)$, and run Algorithm 2 with (correct) parameters α, r . Figure 15 shows the worst, the best, and the median case for each iteration, and illustrates that the convergence (and convergence speed) of the algorithm for the vast majority of cases is independent of the initial point. Moreover, when both rank and sparsity are not too big (sparsity level is 10% or less and rank is 15% or less), we observe very fast convergence.

A.2 Algorithm 3: The effect of the number of observable entries on convergence

In this section, we study convergence properties of Algorithm 3. For different choices of α and r , Figure 16 shows how fast does Algorithm 3 converge to the optimum. We observe extremely fast convergence for both small (< 0.1) and large (≈ 1) fraction of observable entries. However, for medium fractions of observable entries, Algorithm 3 seems to often do not converge. This is an interesting phenomenon that could be studied more deeply in future research. However, for example, as Figure 11 shows, we demonstrate that Algorithm 3 still outperforms the other methods even for the critical medium sized Ω .

A.3 Algorithm 2: Sensitivity to the choice of α and r

In this section we study the sensitivity of Algorithm 2 to the degree at which we choose the rank and sparsity level parameters correctly, compare with their true values at the optimum. We first generate a matrix A as described in Section A.1 for a fixed choice of $\hat{\alpha}, \hat{r}$. We then run Algorithm 2 various choices of α, r , including the correct choice. Figure 17 shows the results. If sparsity and rank levels (α and r) are set to be smaller than their true values at the optimum incorrectly, Algorithm 2 does not converge (as in this case, $\cap \mathcal{X}_i$ might not exist). Moreover, the performance of the algorithm is sensitive to the choice of r , particularly so if we underestimate the true value (see Figure 16). However, overestimating the parameters only leads to a slower convergence.

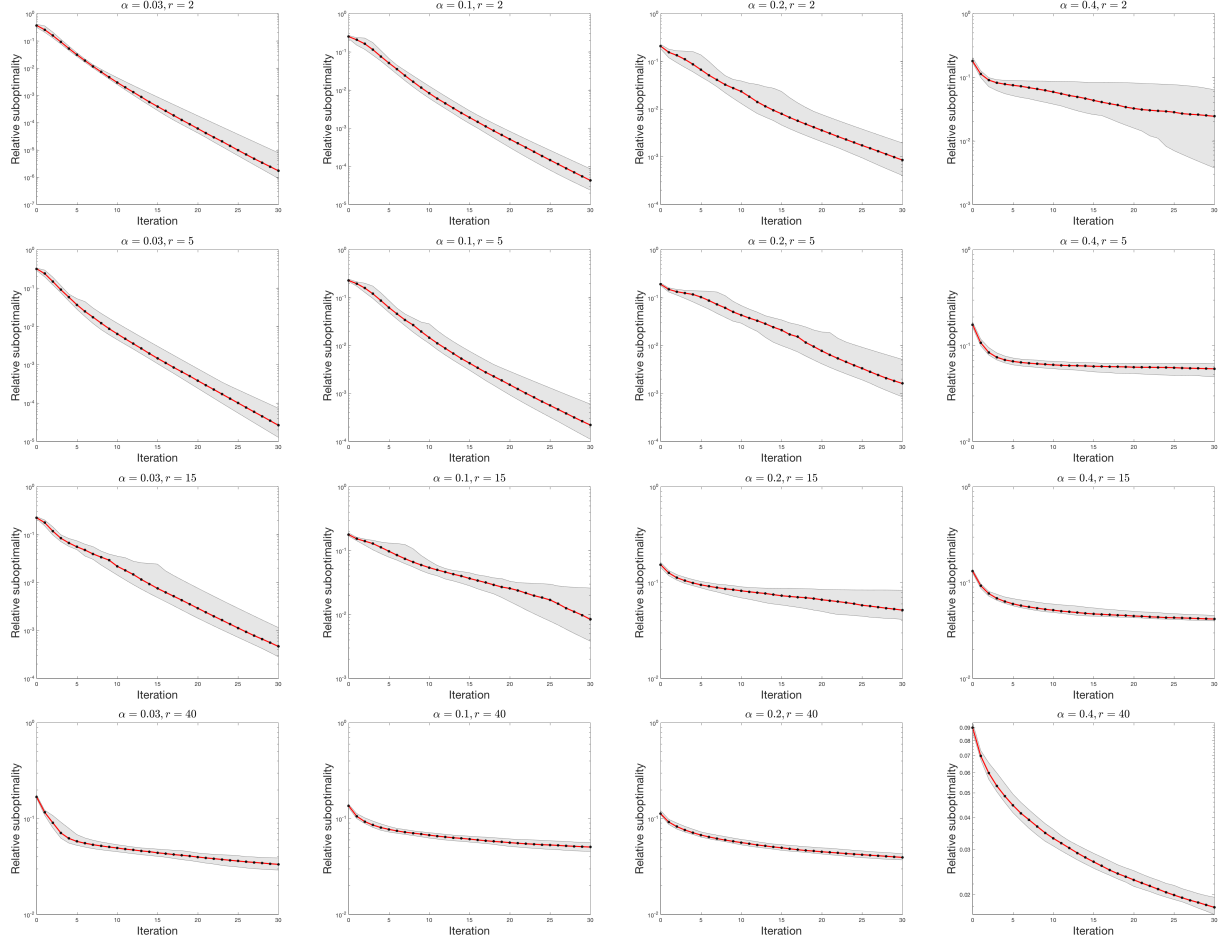


Figure 15: Sensivity of Algorithm 2 to initialization. The best, the worst, and the median case are plotted for each iteration.

B Proof of Lemma 2.1 and Lemma 2.2

We start with proof of Lemma 2.1. Note that for $I \in \mathbb{R}^{mn \times mn}$, $L + S = A$ can be rewritten as

$$\begin{pmatrix} I & I \end{pmatrix} \begin{pmatrix} L \\ S \end{pmatrix} = A.$$

Define $x \stackrel{\text{def}}{=} \text{vec} \begin{pmatrix} L \\ S \end{pmatrix}$ and $\text{vec}(A) = a$. Therefore, the above is equivalent to

$$(I \otimes (I \ I)) x = a,$$

which is just a projection on a particular linear system. Recall that the projection of x_0 in the Frobenius norm (for the vectors it is equivalent to the ℓ_2 norm) onto $\mathcal{A}x = b$ is given as

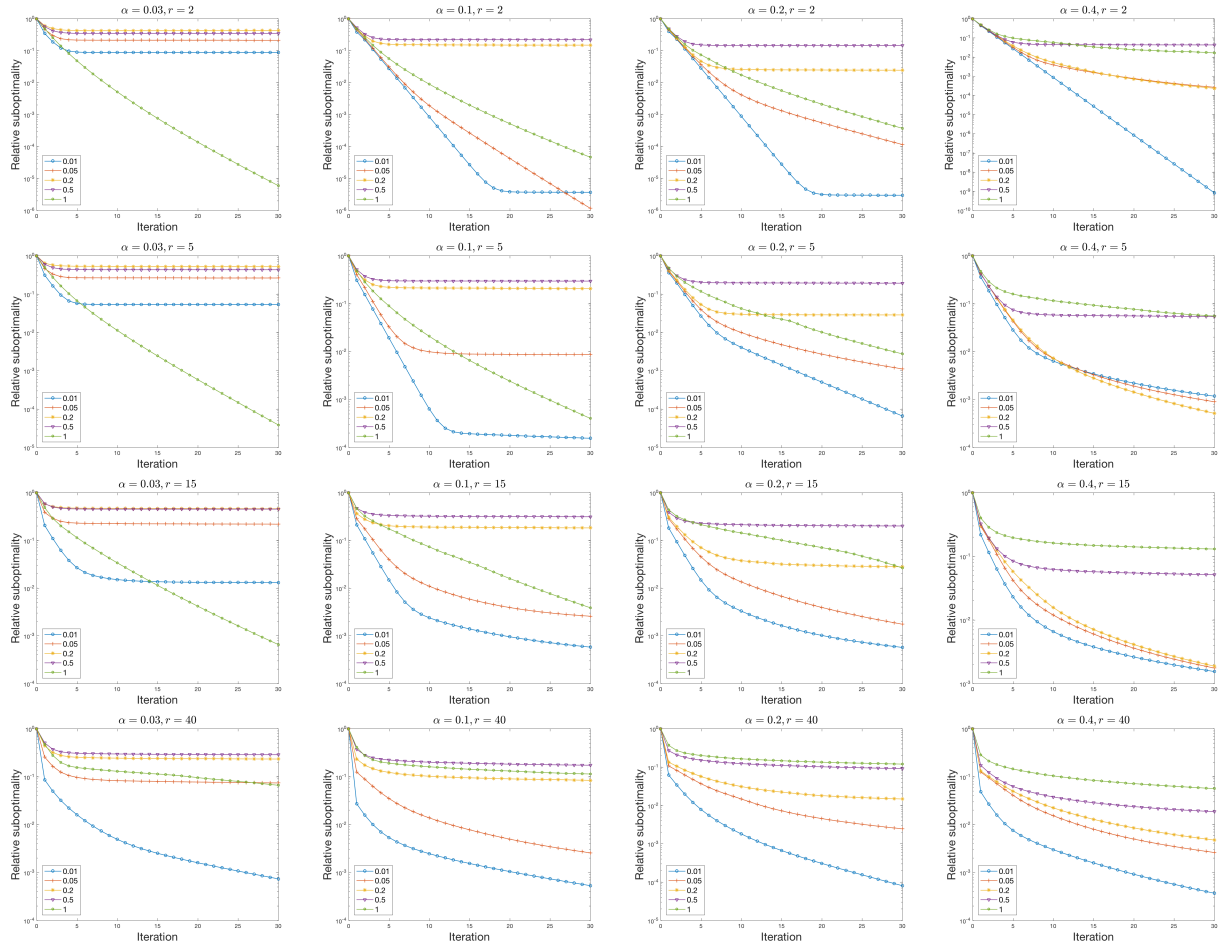


Figure 16: Convergence of Algorithm 3 for several values of Ω . Each line corresponds to a random percentage of the observable entries and shows normalized ℓ_2 norm of $(A - L_k - S_k)_\Omega$.

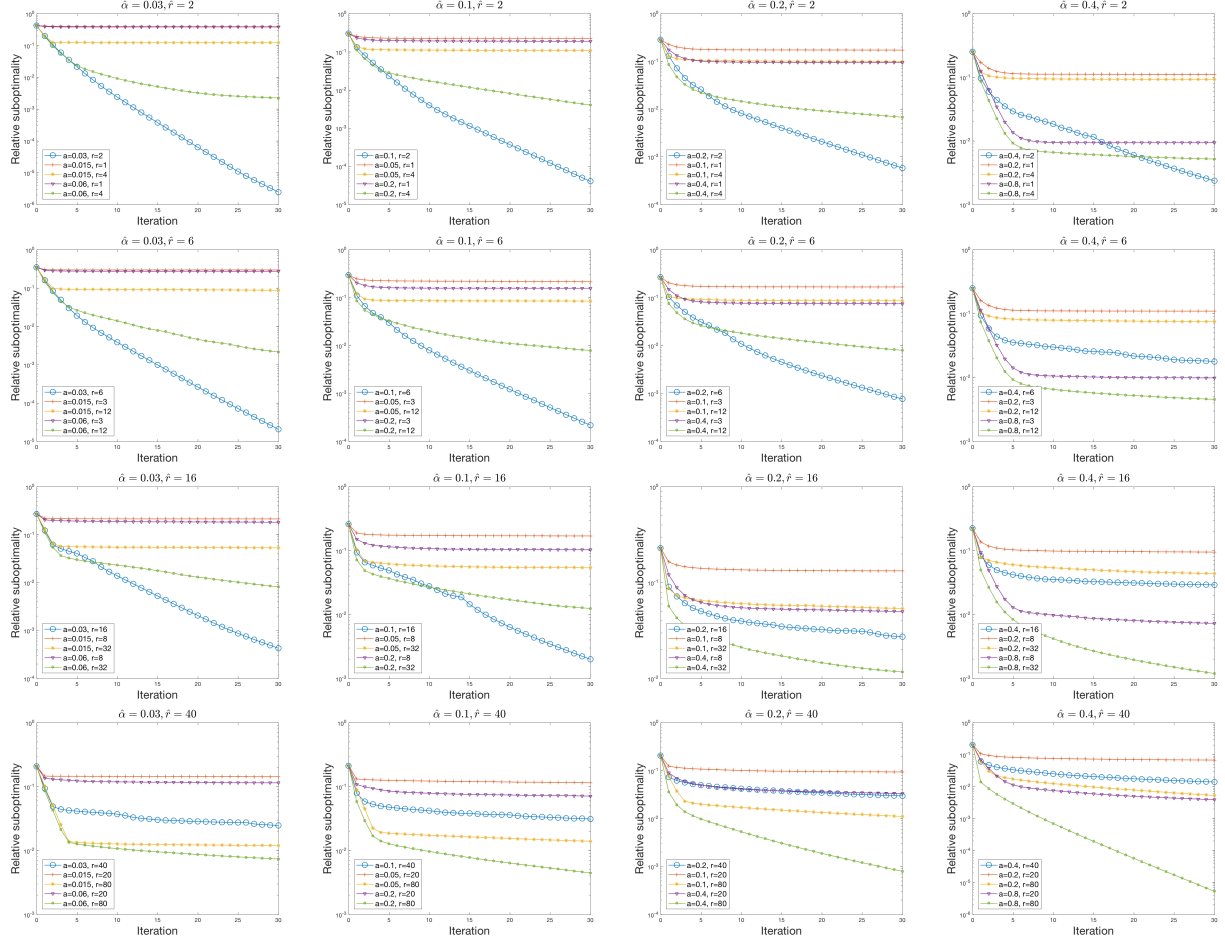


Figure 17: Convergence of Algorithm 3 for the different choices of Ω . Each line corresponds to a random percentage of observable entries and shows normalized ℓ_2 norm of $(A - L_k - S_k)_\Omega$.

$x_0 - \mathcal{A}^\top(\mathcal{A}\mathcal{A}^\top)^\dagger(\mathcal{A}x - b)$. Therefore,

$$\begin{aligned}
x &= x_0 - (I \otimes (I \ I))^\top \left((I \otimes (I \ I)) (I \otimes (I \ I))^\top \right)^\dagger \left((I \otimes (I \ I)) x - a \right) \\
&= x_0 - \frac{1}{2} (I \otimes (I \ I))^\top (I \otimes I) \left((I \otimes (I \ I)) x - a \right) \\
&= x_0 - \frac{1}{2} \left(I \otimes \begin{pmatrix} I & I \\ I & I \end{pmatrix} \right) x + \frac{1}{2} (I \otimes (I \ I))^\top a \\
&= \text{vec} \left(\begin{pmatrix} L_0 \\ S_0 \end{pmatrix} - \frac{1}{2} \begin{pmatrix} L_0 + S_0 \\ L_0 + S_0 \end{pmatrix} + \frac{1}{2} \begin{pmatrix} A \\ A \end{pmatrix} \right),
\end{aligned}$$

which is equivalent to $L^* = \frac{1}{2}(L_0 - S_0 + A)$ and $S^* = \frac{1}{2}(S_0 - L_0 + A)$. Therefore, Lemma 2.1 is established.

To get Lemma 2.2, it remains to note that the problem is coordinate wise separable. Therefore, the solution behaves as in Lemma 2.1. on set Ω , otherwise the coordinates of L, S remain unchanged.

C Two Examples of Convergence

In this section we give two examples of a convex version of the alternating projection method on a problem with similar (block) structure as (9). The first example shows that the convergence might be extremely fast and independent on A , and the second one demonstrates that the rate might not be linear even under convexity.

Example 1. Consider problem (9) with \mathcal{X}_1 defined as (10) and both $\mathcal{X}_2, \mathcal{X}_3$ satisfy the same linear constraint.

Lemma C.1. *Alternating projection algorithm applied on Example 1 converges in 1 iteration.*

Proof. For simplicity, let us vectorize L, S : $x \stackrel{\text{def}}{=} \text{vec}(L), y \stackrel{\text{def}}{=} \text{vec}(S)$ and denote I to be $mn \times mn$ identity matrix. Since the constraints are linear, the alternating projection algorithm applied on them converges as fast as alternating projection applied on any affine translation of them such that nonempty intersection property holds. Let us therefore, without loss of generality consider the following linearly translated problem for some matrix Q :

$$\begin{aligned}\mathcal{X}_1 &\stackrel{\text{def}}{=} \left\{ \begin{pmatrix} x \\ y \end{pmatrix} \mid (I \ I) \begin{pmatrix} x \\ y \end{pmatrix} = 0 \right\} \\ \mathcal{X}_2 &\stackrel{\text{def}}{=} \left\{ \begin{pmatrix} x \\ 0 \end{pmatrix} \mid Qx = 0 \right\} \\ \mathcal{X}_3 &\stackrel{\text{def}}{=} \left\{ \begin{pmatrix} 0 \\ y \end{pmatrix} \mid Qy = 0 \right\}.\end{aligned}$$

Therefore we have for some projection matrix $P = P(Q)$

$$\pi_{\mathcal{X}_2 \cap \mathcal{X}_3} \left(\pi_{\mathcal{X}_1} \begin{pmatrix} x \\ y \end{pmatrix} \right) = \underbrace{\begin{pmatrix} P & 0 \\ 0 & P \end{pmatrix} \begin{pmatrix} \frac{1}{2}I & -\frac{1}{2}I \\ -\frac{1}{2}I & \frac{1}{2}I \end{pmatrix}}_R \begin{pmatrix} x \\ y \end{pmatrix}$$

and the convergence of the algorithm is determined by the maximal eigenvalue of R which is not 0 or 1 in the absolute value. Clearly, vectors of type

$$\begin{pmatrix} p_1 \\ p_1 \end{pmatrix}, \begin{pmatrix} p_2 \\ -p_2 \end{pmatrix}, \begin{pmatrix} p'_1 \\ p'_1 \end{pmatrix}, \begin{pmatrix} p'_2 \\ -p'_2 \end{pmatrix},$$

might form an orthonormal basis of the space for $p_1, p_2 \in \text{Range}(P)$ and $p'_1, p'_2 \perp \text{Range}(P)$. However, each of them is an eigenvector of R with eigenvalue 0 or 1, which finishes the proof. \square

We will now present an example where linear convergence rate cannot be attained.

Example 2. Consider problem (9) for $A \in \mathbb{R}^2$ with \mathcal{X}_1 defined as (10) and both $\mathcal{X}_2, \mathcal{X}_3$ are unit balls.

The next lemma shows that there exist a problem of structure (9), for which alternating projection algorithm does not attain a linear convergence rate.

Lemma C.2. *Suppose that \mathcal{X} is nonempty. There exists a starting point such that for Example 2, alternating projection algorithm does not converge linearly.*

Proof. Choose

$$A = \begin{pmatrix} 2 \\ 0 \end{pmatrix}, \quad L_0 = \begin{pmatrix} \sqrt{2} \\ \sqrt{2} \end{pmatrix}, \quad \text{and} \quad S_0 = \begin{pmatrix} \sqrt{2} \\ -\sqrt{2} \end{pmatrix}.$$

Clearly, in optimum we must have $L^* = e_1, S^* = e_1$. It is a simple exercise to notice that L, S are projected each iteration onto line $x = 1$ and then back to the unit circle. Therefore, alternating projection onto (9) converges as fast as alternating projection onto unit ball and its tangent line. However, it is easy to see that the latter algorithm does not enjoy a linear convergence. \square

D Block Krylov SVD [45]

Algorithm 4: Block Krylov SVD [45] (BKSVD)

- Input** : $L \in \mathbb{R}^{m \times n}$, tolerance $\tilde{\epsilon} \in (0, 1)$, rank $r \leq m, n$
- 1 $q \stackrel{\text{def}}{=} \Theta\left(\frac{\log d}{\sqrt{\tilde{\epsilon}}}\right)$, $\Pi \sim \mathcal{N}(0, 1)^{n \times r}$
 - 2 $K \stackrel{\text{def}}{=} [L\Pi, (LL^\top)L\Pi, \dots, (LL^\top)^q L\Pi]$
 - 3 Orthonormalize the columns of K to obtain $Q \in \mathbb{R}^{m \times qr}$
 - 4 Compute $M \stackrel{\text{def}}{=} Q^\top LL^\top Q \in \mathbb{R}^{qr \times qr}$
 - 5 Set \bar{U}_r to the top r singular vectors of M
 - 6 **Output** : $Z = Q\bar{U}_r$
-